Journal of Molecular Structure 1052 (2013) 67–75

Contents lists available at ScienceDirect

Journal of Molecular Structure

journal homepage: www.elsevier.com/locate/molstruc

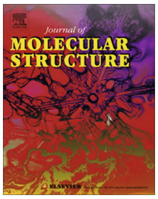

Studies on molecular structure, spectral analysis, chemical reactivity and first hyperpolarizability of a newly synthesized 1,9-bis[(4-isonicotinoyl)-hydrazonomethyl]-5-phenyl-dipyrromethane using experimental and theoretical approaches

R.N. Singh *, Amit Kumar, Poonam Rawat, R.K. Tiwari, Ashok Kumar Singh

Department of Chemistry, University of Lucknow, Lucknow 226007, U.P., India

HIGHLIGHTS

- FT-IR spectrum of the studied compound was recorded and compared with the theoretical result.
- To determine the hyperconjugative interactions NBO analysis was performed.
- Theoretical calculated (β_0) indicates the NLO response of the investigated molecule.

ARTICLE INFO

Article history:
Received 1 June 2013
Received in revised form 16 August 2013
Accepted 20 August 2013
Available online 4 September 2013

Keywords:
Thermochemistry
TD-DFT
NBO analysis
Reactivity descriptor
NLO

ABSTRACT

The detailed spectroscopic analysis of a newly synthesized dipyrromethane derivative: 1,9-bis[(4-isonicotinoyl)-hydrazonomethyl]-5-phenyl-dipyrromethane (**3**) has been performed using experimental measurement and quantum chemical calculations. Calculated thermodynamic parameters (H, G, S) of all the reactants and products have been used to determine the nature of reaction of synthesis. Occurring of a ^{1}H NMR singlet at 5.54 ppm indicates *meso*-proton and formation of product molecule (**3**). The molecular orbital coefficients and molecular plots analysis indicates the nature of electronic excitations as $\pi \rightarrow \pi^*$. Natural bond orbitals (NBOs) analysis has been carried out to investigate the intramolecular interactions within molecule and their second order stabilization energy. The primary hyperconjugative interactions $n_2(\text{O23}) \rightarrow \sigma^*(\text{N21—C22})/\sigma^*(\text{C22—C24})$ and $n_2(\text{O48}) \rightarrow \sigma^*(\text{N46—C47})/\sigma^*(\text{C47—C49})$ stabilize the molecule to a greater extent ~117.75 KJ/mol. Global electrophilicity index ($\omega = 3.64$ eV) shows that the title molecule (**3**) is a strong electrophile. Local reactivity descriptors: Fukui functions (f_k^+, f_k^-), local softnesses (s_k^+, s_k^-) and electrophilicity indices (ω_k^+, ω_k^-) analyses were performed to find out the reactive sites within molecule. The first hyperpolarizability (β_0) has been computed and found to be 60.95×10^{-30} esu indicating synthesized molecule to be suitable for non-linear optical response.

1. Introduction

Dipyrromethanes (DPM) are the building blocks for the syntheses of a variety of calix[n] pyrroles, porphyrins [1–4], polypyrrolic macrocycles [5], hexaphyrin [6] and corroles [7,8]. The oxidized dipyrromethanes (dipyrromethenes or dipyrrins) give monoanionic, conjugated, planar ligands that have attracted attention in the metal organic framework due to strong coordinating ability towards different metal ions [9–12]. They are versatile ligands for supramolecular coordination chemistry and self-assembly with various transition metal ions [13,14]. The dipyrrinato metal complexes are used for developing novel magnetic, electronic [15–19], luminescent [20] and strong optical absorption materials [20,21]. DPM based amido-imine hybrid macrocycles have shown oxoanions receptor property [22]. Dipyrrins are also used as ligands for the syntheses of boron dipyrromethene (BODIPY) [23–25], which are used extensively as molecular probes and dyes.

Hydrazide–hydrazones having frame —CO—NH—N=CH— are versatile intermediates for the syntheses of *N*-alkyl hydrazides, 1,3,4-oxadiazolines, 2-azetidinones and 4-thiazolidinones [26,27]. These compounds show different biological activities such as antidepressant [28], antimalarial [29], anticancer [30] and antimicrobial [31] due to the presence of the active pharmacophore (—CO—NH—N=CH—). They are used as prospective new materials for the development of potential chemosensors [32],

---

* Corresponding author. Tel.: +91 9451308205.
E-mail address: rnsvk.chemistry@gmail.com (R.N. Singh).

0022-2860/$ - see front matter © 2013 Elsevier B.V. All rights reserved.
http://dx.doi.org/10.1016/j.molstruc.2013.08.037

opto-electronic [33] and non-linear optical (NLO) response [34]. The development of organic NLO materials for device applications requires multidisciplinary effort involving both theoretical and experimental studies. Quantum-chemical calculations have made an important contribution to the understanding of the electronic polarization underlying the molecular NLO processes and the establishment of structure–property relationships [35,36]. Organic molecules with large second-order NLO are the subject of substantial research due to their potential applications in optical modulation, molecular switching, optical memory, and frequency doubling [37–42]. Nonlinearity in organic molecules can be synthetically modulated by varying the composition or length of conjugated π-systems, and by evaluating the effects of various electron-donor and -acceptor groups. Although, organic molecules are not as robust as inorganics, they have received a great deal of interest in the non-linear optics field and they offer many advantages over traditional inorganic crystals: (i) organic materials show high molecular hyperpolarizability and fast response time; (ii) they are cheaper to produce and easier to fabricate; and (iii) their structures can be modified in numerous ways allowing to finely tune NLO properties for desired applications.

In observation of above applications of dipyrromethanes and hydrazide–hydrazones, hydrazide–hydrazones containing dipyrromethane: 1,9-bis[(4-isonicotinoyl)-hydrazonomethyl]-5-phenyl-dipyrromethane (**3**) has been synthesized and characterized using experimental measurement (^{1}H NMR, UV–Visible, FT-IR, Mass spectroscopic techniques) and quantum chemical calculations. The nature of chemical reactivity and site selectivity of this molecule has been determined on the basis of Global and Local reactivity descriptors. The first hyperpolarizability (β_0) has been computed to indicate suitability for non-linear optical response.

2. Experimental details

2-[(4-Isonicotinoyl)-hydrazonomethyl]-1*H*-pyrrole (**1**) was prepared by stirring the equimolar reaction mixture of pyrrole-2-carboxaldehyde and isonicotinic acid hydrazide at room temperature. Benzaldehyde (**2**) was purchased from commercial source. The Mass spectrum of (**3**) was recorded on JEOL-Acc TDF JMS-T100LC, Accu TOF mass spectrometer. The ^{1}H NMR spectrum of (**3**) was recorded in MeOD on Bruker DRX-300 spectrometer using TMS as an internal reference. The FT-IR spectrum was recorded in KBr medium on a Bruker spectrometer. The UV–Visible absorption spectrum of (**3**), (1×10^{-5} M in MeOD) was recorded on ELICO SL-164 spectrophotometer.

2.1. Synthesis of 1,9-bis[(4-isonicotinoyl)-hydrazonomethyl]-5-phenyl-dipyrromethane (3)

To the solution of 2-[(4-isonicotinoyl)-hydrazonomethyl]-1*H*-pyrrole (0.200 g, 0.93420 mmol) and benzaldehyde (0.0495 g, 0.047 ml, 0.46713 mmol) in 25 ml methanol conc. HCl (0.001 ml) was added as catalyst. The reaction mixture was refluxed for 12 h; the color of reaction was changed to dark brown. The completion of reaction was monitored by thin layer chromatography (TLC). Now, the reaction mixture was treated with saturated aqueous solution of sodium bicarbonate ($NaHCO_3$) and extracted with dichloromethane (30 ml × 4). The organic layer was dried over $MgSO_4$ and solvent was removed under reduced pressure. The formed solid was purified by column chromatography using hexane, dichloromethane as eluent and the pure product (**3**) was obtained. Color: dark brown; Yield: 67.50%; MS for $C_{29}H_{24}N_8O_2$: Calcd. 516.20 amu, Obs. *m*/*z* 517.21 [M$^+$ + 1]. Elemental analysis for $C_{29}H_{24}N_8O_2$: Calcd. C 67.41, H 4.68, N 21.70, Obs. C 67.38, H 4.72, N 21.67%.

3. Quantum chemical calculations

All the quantum chemical calculations have been carried out with Gaussian 09 program package [43] using DFT method, B3LYP functional and 6-31G(d,p) basis set to predict the molecular structure, ^{1}H NMR chemical shifts, vibrational wavenumbers, electronic transitions, electronic reactivity descriptors and first hyperpolarizability. B3LYP invokes Becke's three parameter (local, non local, Hartree–Fock) hybrid exchange functional (B3) [44], with Lee–Yang–Parr correlational functional (LYP) [45]. The basis set 6-31G(d,p) with 'd' polarization functions on heavy atoms and 'p' polarization functions on hydrogen atoms are used for better description of polar bonds of molecule [46,47]. The 'p' polarization functions on hydrogen atoms are used for reproducing the out of plane vibrations involving hydrogen atoms. The motivation to use B3LYP functional and the bases set 6-31G (d,p) for the theoretical calculations is due to ability to successfully predict a wide range of molecular properties of hydrogen bonded complexes at a relatively low computational cost. To estimate the enthalpy (*H*) and Gibbs free energy (*G*) values, thermal corrections to the enthalpy and Gibbs free energy are added to the calculated total energies. Time dependent density functional theory (TD-DFT) is used to find the various electronic excitations and their nature within molecule. The second-order Fock matrix was used to evaluate the donor–acceptor interactions in the NBO basis [48]. For each donor (i) and acceptor (j), the stabilization energy $E(2)$ associated with the delocalization $i \to j$ is estimated using equation [49,50] as:

$$E(2) = \Delta E_{ij} = q_i((F(i,j)^2/(\varepsilon_j - \varepsilon_i')))$$

where q_i is the donor orbital occupancy, ε_i and ε_j are diagonal elements and $F(i, j)$ is the off-diagonal NBO Fock matrix element between i and j NBO orbitals.

Potential energy distribution along internal coordinates has been calculated by Gar2ped software [51]. Global reactivity descriptors [52–56]: electronegativity (χ), chemical potential (μ), global hardness (η), global softness (S) and electrophilicity index (ω) are highly successful in predicting global reactivity trends and calculated using the following equations: $\chi = -1/2(\varepsilon_{\text{LUMO}} + -\varepsilon_{\text{HOMO}})$; $\mu = 1/2\ (\varepsilon_{\text{LUMO}} + \varepsilon_{\text{HOMO}})$; $\eta = 1/2\ (\varepsilon_{\text{LUMO}} - \varepsilon_{\text{HOMO}})$; $S = 1/2\eta$; $\omega = \mu^2/2\eta$. The local reactivity descriptors [52,56] such as Fukui functions $f_k^+(r)$, $f_k^-(r)$, $f_k^0(r)$ calculated using the following equations: $f_k^+(r) = [\rho_{N+1}(r) - \rho_N(r)] = [q_k(N+1) - q_k(N)]$, for nucleophilic attack; $f_k^-(r) = [\rho_N(r) - \rho_{N-1}(r)] = [q_k(N) - q_k(N-1)]$, for electrophilic attack; $f_k^0(r) = 1/2[\rho_{N+1}(r) + \rho_{N-1}(r)] = 1/2[q_k(N+1) + q_k(N-1)]$, for radical attack, where, ρ is the electron density of atom k in the molecule, q is the gross charge of atom k in the molecule and N, $N + 1$, $N - 1$ are electron systems containing neutral, anion, cation form of molecule, respectively. Using Fukui functions, other local reactivity descriptors: local softnesses ($s_k^+,\ s_k^-,\ s_k^0$) and electrophilicity indices ($\omega_k^+,\ \omega_k^-,\ \omega_k^0$) are calculated using following equations: $s_k^+ = Sf_k^+,\ s_k^- = Sf_k^-,\ s_k^0 = Sf_k^0;\ \omega_k^+ = \omega f_k^+,\ \omega_k^- = \omega f_k^-,\ \omega_k^0 = \omega f_k^0$, where; +, – and 0 sign show nucleophilic, electrophilic and radical attack, respectively.

The total static dipole moment (μ_0), mean polarizability ($|\alpha_0|$), anisotropy of polarizability ($\Delta\alpha$) and first hyperpolarizability (β_0) are calculated using x, y, z components by following equations [57–60]

$$\mu_0 = (\mu_x^2 + \mu_y^2 + \mu_z^2)^{1/2}$$

$$|\alpha_0| = 1/3(\alpha_{xx} + \alpha_{yy} + \alpha_{zz})$$

$$\Delta\alpha = 2^{-1/2}[(\alpha_{xx} - \alpha_{yy})^2 + [(\alpha_{yy} - \alpha_{zz})^2 + (\alpha_{zz} - \alpha_{xx})^2 + 6\alpha_{xx}^2]^{1/2}$$

$$\beta_0 = [(\beta_{xxx} + \beta_{xyy} + \beta_{xzz})^2 + (\beta_{yyy} + \beta_{xxy} + \beta_{yzz})^2 + (\beta_{zzz} + \beta_{xxz} + \beta_{yyz})^2]^{1/2}$$

where the conversion factors for $|\alpha_0|$ and $\Delta\alpha$ is1 a.u. = 0.1482×10^{-24} esu; for β_0 1 a.u = 0.008639×10^{-30} esu.

4. Results and discussion

4.1. Thermochemistry

For simplicity, the reactants 2-[(4-isonicotinoyl)-hydrazonomethyl]-1*H*-pyrrole and benzaldehyde are abbreviated as (**1**), (**2**) and product 1,9-bis[(4-isonicotinoyl)-hydrazonomethyl]-5-phenyl-dipyrromethane, byproduct water as (**3**), (**4**), respectively. The calculated thermodynamic parameters enthalpy (*H*), Gibbs free energy (*G*) and entropy (*S*) of **(1), (2), (3), (4)** and their change (ΔH, ΔG, ΔS) for Reaction, at 25 °C are listed in Table 1. The calculated negative values of enthalpy change (ΔH) and entropy change (ΔS) show that energy factor is favorable, whereas entropy factor is unfavorable for formation of the product. It is to be noticed that net spontaneity of the chemical reaction is depend upon the Gibbs free energy change of reaction (ΔG). For uncatalyzed reaction, the calculated positive value of (ΔG) shows that this reaction is non-spontaneous at 25 °C. Therefore, this reaction is carried out in presence of acid as catalyst.

4.2. Molecular geometry

Optimized geometry of all the reactants (**1**, **2**) and product (**3, 4**) involved in chemical reaction is shown graphically in Supplementary Scheme 1. Optimized geometry for the ground state lower energy conformer of (**3**) is shown in Fig. 1. Selected optimized geometrical parameters of (**3**), calculated at B3LYP/6-31G (d,p) are listed in Supplementary Table 1. The ground state lower energy conformer of (**3**) possesses C_1 symmetry. In (**3**), two pyrrole units in *anti* form gives lower energy conformer. The *anti* form of two pyrrole units is also well reported in the crystal structure of dipyrromethane derivatives [61,62]. The *E*-configuration about the Schiff base bonds as C19═N20, C44═N45 with respect to the Ar—CO—NH— group and pyrrole give lower energy conformer. The *E*-configuration about the Schiff base bonds is also well reported in the crystal structure of hydrazone derivatives [63,64]. The asymmetry in the N14—C18 and N14—C15 bond lengths is explained due to the presence of the two different groups as 4-isonicotinoyl-hydrazonomethyl at C18 and substituted methylene group at C15 carbon atom of pyrrole ring. In same manner, the asymmetry of the N39—C43 and N39—C40 bonds is also explained due to the presence of the two different groups at C43 and C40 carbon atoms of pyrrole ring. The *meso*-substituted DPM molecule (**3**) is associated with the C1 as tetrahedral (sp^3) carbon atom. The angles associated with C1 carbon atom as C15C1C2, C40C1C2, C15C1H8, C40C1H8 are deviated from the ideal tetrahedral angle and have values in the range 105.92–114.00.

4.3. ^{1}H NMR spectroscopy

The geometry of the title compound, together with that of tetramethylsilane (TMS) is fully optimized. ^{1}H NMR chemical shifts are calculated with GIAO approach at B3LYP/6-31G(d,p) method [65]. Chemical shift of any '*x*' proton (δ_X) is equal to the difference between isotropic magnetic shielding (IMS) of TMS and proton (*x*). It is defined by the equation: $\delta_X = \mathrm{IMS}_{\mathrm{TMS}} - \mathrm{IMS}_X$. The experimental ^{1}H NMR spectrum of (**3**) is shown in Fig. 2. The calculated and experimental ^{1}H NMR chemical shifts (δ/ppm) for (**3**), in MeOD solvent at 25 °C are given in Table 2. The observed singlet chemical shifts at 8.388, 9.452 ppm for Schiff base —C<u>H</u>═N and ArCON<u>H</u>, respectively indicates formation of aroylhydrazone linkage (—CH═N—NH—CO—Ar) in the title molecule. The observed chemical shift as a singlet at 5.544 ppm indicates presence of *meso*-proton i.e. formation of dipyrromethane molecule. In order to compare the chemical shifts, correlation graphs between the experimental and calculated ^{1}H NMR chemical shifts are shown in Supplementary Fig. 2. The correlation graph follows the linear equation: $y = 1.03x - 0.152$, where '*x*' is the calculated ^{1}H NMR chemical shift, '*y*' is the experimental ^{1}H NMR chemical shift (δ in ppm). The correlation value ($R = 0.91$) shows that there is an agreement between experimental and calculated chemical shifts.

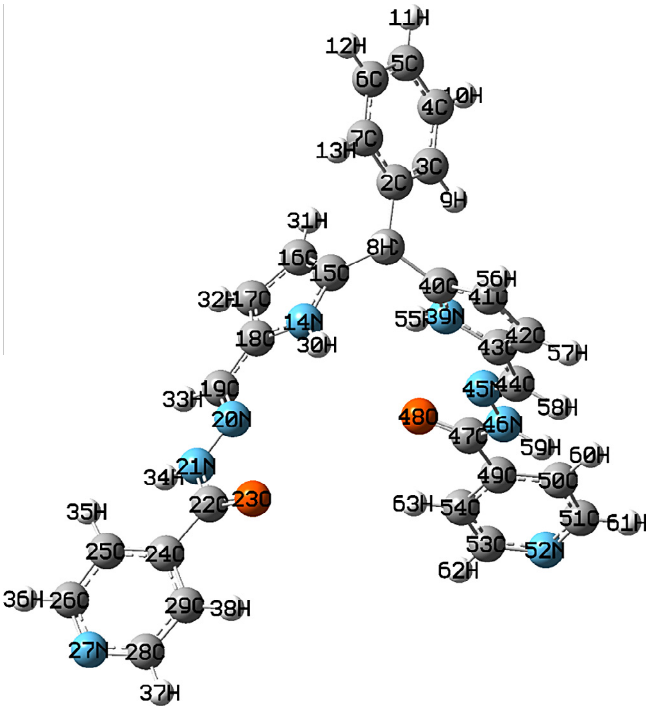

Fig. 1. Optimized geometry for the ground state lower energy conformer of (**3**).

Table 1
Calculated thermodynamic parameters: enthalpy (*H*/a.u.), Gibbs free energy (*G*/a.u.) and entropy [*S*/(cal/mol K)] of (**1**), (**2**), (**3**), (**4**) and their change for **reaction**, at 25 °C.

	(**1**)	(**2**)	(**3**)	(**4**)		**Reaction**
H	−719.1875	−345.4654	−1707.4572	−76.3945	ΔH	−0.0111
G	−719.2439	−345.5031	−1707.5656	−76.4160	ΔG	0.0093
S	118.575	79.467	228.287	45.116	ΔS	−43.214

4.4. UV–Visible spectroscopy

The nature of the excitations in the observed UV–Visible spectrum of the title compound has been studied by the time dependent density functional theory (TD-DFT). The calculated electronic excitations of high oscillatory strength and experimental are listed in Table 3. The comparison between experimental and theoretical UV–Visible spectra for (**3**) is shown in Fig. 3. HOMO–LUMO and their vicinal molecular orbital plots involved in the high oscillator strength electronic excitations for (**3**) are shown in Supplementary Fig. 3. The HOMO–LUMO energy gap for (**3**) is found to be 3.64 eV. A combined experimental and theoretical UV–Visible spectrum analysis of (**3**) indicates that the first observed electronic excitation at $\lambda_{max} = 278$ nm agrees well with the aggregate of two electronic excitations calculated at $\lambda_{max} = 278.4$, $f = 0.218$ and $\lambda_{max} = 282.6$ nm, $f = 0.246$. The second observed λ_{max} at 356 nm corresponds to the aggregate of three electronic excitations calculated at $\lambda_{max} = 361.9$, $f = 0.229$, $\lambda_{max} = 379.9$ nm, $f = 0.229$ and

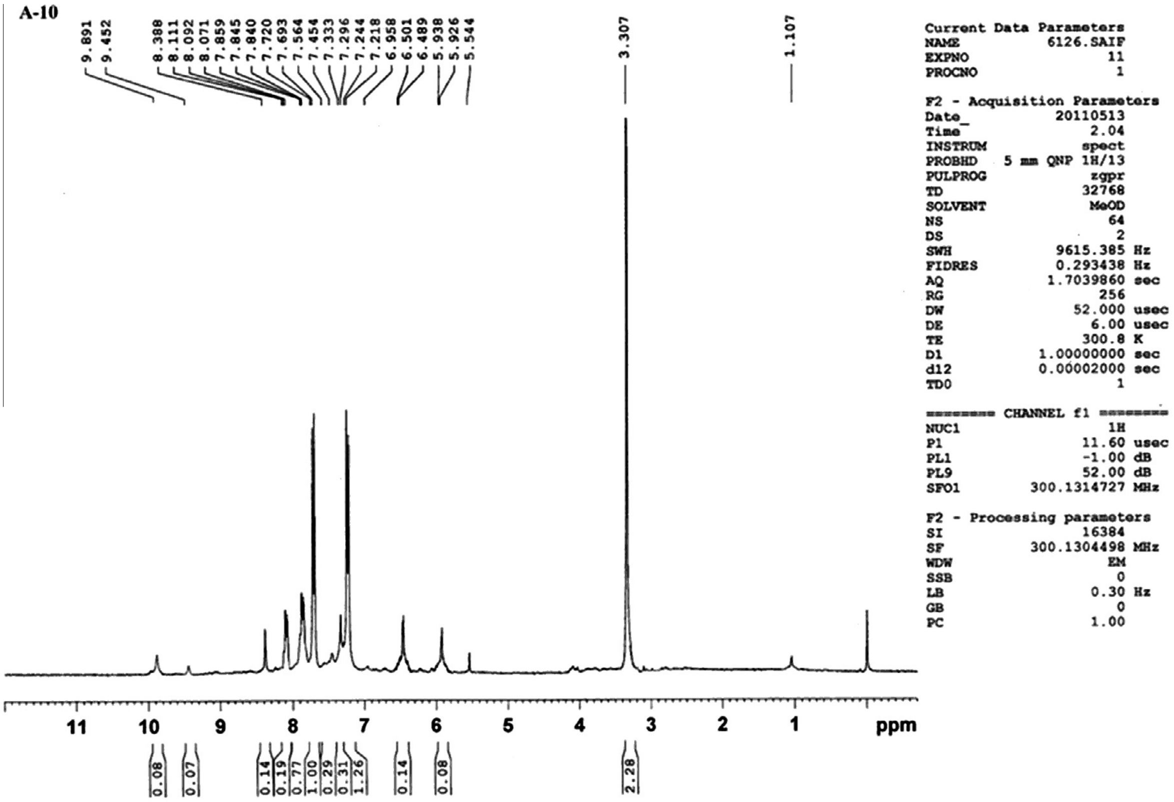

```
Current Data Parameters
NAME             6126.SAIF
EXPNO                   11
PROCNO                   1

F2 - Acquisition Parameters
Date_             20110513
Time                  2.04
INSTRUM              spect
PROBHD   5 mm QNP 1H/13
PULPROG               zgpr
TD                   32768
SOLVENT               MeOD
NS                      64
DS                       2
SWH            9615.385 Hz
FIDRES         0.293438 Hz
AQ            1.7039860 sec
RG                     256
DW               52.000 usec
DE                 6.00 usec
TE                300.8 K
D1           1.00000000 sec
d12          0.00002000 sec
TD0                      1

======== CHANNEL f1 ========
NUC1                    1H
P1                11.60 usec
PL1               -1.00 dB
PL9               52.00 dB
SFO1        300.1314727 MHz

F2 - Processing parameters
SI                   16384
SF          300.1304498 MHz
WDW                     EM
SSB                      0
LB                 0.30 Hz
GB                       0
PC                    1.00
```

Fig. 2. The experimental ^{1}H NMR chemical shifts for (**3**).

Table 2
Calculated and experimental ^{1}H NMR chemical shifts (δ/ppm) in MeOD at 25 °C for (**3**).

Atom no.	δ_{calcd}	δ_{exp}	Assignment
H 8	5.7768	5.544	(s, 1H, *meso*-CH)
H 9	7.3044	7.218–7.564	(m, 5H, benzene-CH)
H10	7.6378		
H11	7.615		
H12	7.7024		
H13	7.6379		
H30	9.2936	9.891	(s, 2×1H, pyrrole-NH)
H31	5.7919	5.926–5.938	(s, 2×1H, pyrrole-CH)
H32	6.6341	6.489–6.501	(s, 2×1H, pyrrole-CH)
H33	7.8272	8.388	(s, 2×1H, —CH═N)
H34	9.2228	9.452	(s, 2×1H, ArCONH)
H35	7.8015	7.840–7.859	(s, 2×2H, pyridine-CH)
H38	8.0504		
H36	9.0276	8.071–8.111	(s, 2×2H, pyridine-CH)
H37	9.0556		
H55	8.6406	9.891	(s, 2×1H, pyrrole-NH)
H56	6.4346	5.926–5.938	(s, 2×1H, pyrrole-CH)
H57	6.7594	6.489–6.501	(s, 2x1H, pyrrole-CH)
H58	7.7888	8.388	(s, 2×1H, —CH═N)
H59	9.156	9.452	(s, 2×1H, ArCONH)
H60	7.7869	7.840–7.859	(s, 2×2H, pyridine-CH)
H63	8.0328		
H61	9.0019	8.071–8.111	(s, 2×2H, pyridine-CH)
H62	9.0297		

Table 3
Calculated and experimental electronic transitions for (**3**): E/eV, oscillatory strength (f), (λ_{max}/nm) at TD-DFT/B3LYP/6-31G(d,p) level.

S. no.	Excitations	E (eV)	(f)	λ_{max} calcd.	λ_{max} obs.	Assignment
1.	135 → 140, H → L + 4	4.45	0.218	278.4	278	$\pi \to \pi^*$
	134 → 138, H − 1 → L + 2	4.38	0.246	282.6		
2.	134 → 136, H − 1 → L	3.42	0.229	361.9	356	$\pi \to \pi^*$
	135 → 137, H → L + 1	3.26	0.229	379.9		
	135 → 136, H → L	3.19	0.369	387.8		

λ_{max} = 387.8 nm, f = 0.369. Therefore, the observed λ_{max} are blue shifted up to ~32 nm compared with the calculated λ_{max} in the theoretical UV–Visible spectrum. According to TD-DFT calculations the observed bands at 278, 356 nm originate mainly due to H → L + 4, H − 1 → L + 2; H − 1 → L, H → L + 1, H → L excitations, respectively. The molecular orbital H, H − 1 are localized over C4—C5, C2—C3 of pyrrole ring, whereas L, L + 1, L + 2, L + 4 are localized over C26—N27, C50—C51 of pyridine, C19—N20 of Schiff base, C24—C25 of pyridine ring, respectively. On the basis of molecular orbital coefficients and molecular orbital plots analyses, the nature of both electronic excitations is assigned as $\pi \to \pi^*$.

4.5. Natural bond orbitals (NBOs) analysis

Natural bond orbital (NBO) analysis is an important tool for studying hybridization, covalency, hydrogen-bonding and van der Waals interactions [66,67]. Second-order perturbation theory analysis of the Fock matrix in NBO basis for (**3**) is presented in Supplementary Table 2. The interactions π(C15—C16) → π^*(C17—C18), π(C17—C18) → π^*(C15—C16) and n_1(N14) → π^*(C15—C16)/π^*(C17—C18) are responsible for the conjugation of respective π-bonds in pyrrole ring due to the high electron density at π bonds (1.755–1.780) or loan pair (1.575) and low density at π^* bonds (0.361–0.401) and stabilized the molecule with energy in the region 75.57–173.39 kJ/mol. The interactions n_1(N14) → π^*(C15—C16)/π^*(C17—C18) indicate the involvement of loan-pair of pyrrole N atom with π-electron delocalization in ring. In same manner, for other pyrrole unit the conjugation of π-bonds, and

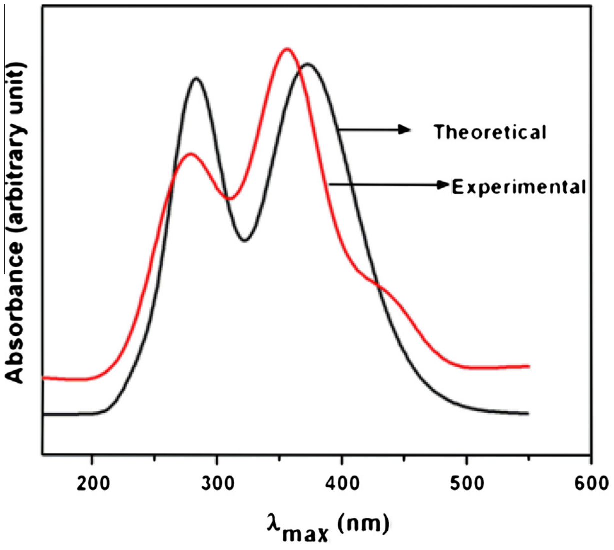

Fig. 3. Correlation graph between experimental and calculated ^{1}H NMR chemical shifts for (**3**).

involvement of loan-pair of pyrrole N atom with π-electron delocalization in ring can be explained. The interactions π(C17—C18) → π^*(C19—C20), π(C19—C20) → π^*(C17—C18) demonstrate the conjugation of these bonds with C18—C19 and stabilized the molecule up to ~95.38 kJ/mol. The interactions π(C2—C3) → π^*(C4—C5)/π^*(C6—C7), π(C4—C5) → π^*(C2—C3)/π^*(C6—C7) and π(C6—C7) → π^*(C2—C3)/π^*(C4—C5) are responsible for the conjugation of respective π-bonds in benzene ring. In same way, $\pi \rightarrow \pi^*$ interactions in pyridine ring designate conjugation of π-bonds in ring and stabilized the molecule with maximum energy ~111.98 kJ/mol. It is to be noticed that the charge transfer interactions are formed by the orbital overlap between bonding (π) and antibonding (π^*) orbitals, which results in intramolecular charge transfer (ICT) causing stabilization of the system. The movement of π-electron cloud from donor to acceptor i.e. intramolecular charge transfer (ICT) can make the molecule more polarized which is responsible for the NLO properties of molecule. Therefore, the title compound may be used in non-linear optical materials.

The primary hyperconjugative interactions n_2(O23) → σ^*(N21—C22)/σ^*(C22—C24) and n_2(O48) → σ^*(N46—C47)/σ^*(C47—C49) are stabilized the molecule with maximum energy ~117.75 kJ/mol. The other interactions n_1(N21) → π^*(C22—O23) and n_1(N46) → π^*(C47—O48) are also stabilized the molecule to a greater extent ~216.61 kJ/mol. The secondary hyperconjugative interactions $\sigma \rightarrow \sigma^*$ associated with benzene, pyrrole, and pyridine ring are stabilized the molecule with maximum energy ~15.75, 25.79, 16.38 kJ/mol, respectively.

Selected Lewis orbitals (occupied bond or lone pair) of (**3**) with NBO hybrids are listed in Supplementary Table 3. The NBO hybrids analysis shows that all the N—H/C—N bond orbitals are polarized towards the nitrogen atom (ED = 59.34 – 73.87% at N) and C—O bond orbitals towards oxygen atom (ED = 64.92 – 64.93% at O). The electron density distribution around the loan pair of O, N atoms and imino group (>NH) also influences the polarity of the compound. Therefore, they consist with the maximum electron density on the oxygen and nitrogen atoms, which is responsible for the polarity of molecule.

4.6. Vibrational assignments

The theoretical (selected) and experimental vibrational wavenumbers of (**3**) and their assignments using PED are given in Table 4. Comparison among experimental and theoretical (selected) IR spectra for (**3**) in the region 4000–400 cm^{-1} is shown Fig. 4. The total number of atoms (*n*) in monomer (**3**) is 63, therefore this gives 183, (3*n* – 6) vibrational modes. The calculated wavenumbers are scaled down using scaling factor 0.9608 [68], to discard the anharmonicity present in real system. The observed wavenumbers are assigned by comparing the calculated wavenumbers using potential energy distribution (PED) analysis of the various vibrational modes.

4.6.1. N—H vibrations

In the experimental FT-IR spectrum of (**3**), the N—H stretches of pyrrole ($\nu_{N—H}$) is observed at 3425 cm^{-1}, whereas it is calculated at 3506 cm^{-1} in one pyrrole unit and at 3492 cm^{-1} in other pyrrole unit. The observed wavenumber at 3425 cm^{-1} also corresponds to the N—H stretch of pyrrole at 3475 cm^{-1}, reported in literature [69]. The calculated wavenumber at 584 cm^{-1} depicts the presence of N—H wagging mode of pyrrole and observed at 567 in the experimental FT-IR spectrum. The N—H stretches of ArCONH part of molecule is observed at 3286 cm^{-1}, whereas it is calculated at 3382 cm^{-1} in the experimental FT-IR spectrum. The observed deformation mode of hydrazide N—H at 1496 cm^{-1} matches well with the calculated wavenumber at 1503 cm^{-1}. The observed band at 1496 cm^{-1} also corresponds to the N—H deformation of hydrazide at 1506 cm^{-1}, reported in literature [70].

4.6.2. C—H vibrations

The C—H stretching vibrations of pyrrole and benzene rings are assigned in the region 3136–3122, 3085–3078 cm^{-1}, respectively in theoretical IR-spectrum. The calculated C—H stretches of pyridine at 3049 cm^{-1} match well with the observed wavenumber at 3052 cm^{-1} experimentally. These $\nu_{C—H}$ vibrations also correspond to the C—H stretching vibrations for aromatic compounds reported in literature in the region 3100–3000 cm^{-1} [71,72]. The calculated wavenumber at 2941 cm^{-1} exhibits the presence of C—H stretching of Schiff base and observed at 2923 cm^{-1} in the experimental FT-IR spectrum. The C—H stretching associated with C1 as tetrahedral carbon atom ($\nu_{C1—H8}$) is observed at 2852 cm^{-1}, whereas it is calculated at 2910 cm^{-1} in theoretical IR-spectrum. In substituted benzene rings, the aromatic C—H stretching vibrations (Ar-ν_{CH}), in-plane ("ip") and out-of-plane ("oop") C—H bending vibrations are reported in literature in the region 3000–3100, 1300–1000 and 900–675 cm^{-1}, respectively [71]. The C—H stretching vibrations associated with benzene, pyridine and pyrrole ring are assigned at 1312, 1302, 1286 cm^{-1}, respectively. The calculated wavenumbers at 1315, 914 cm^{-1} designate the in-plane and out-of-plane C—H deformation of Schiff base, respectively and correspond to the observed wavenumber at 1287, 910 cm^{-1}. The wagging modes (an out-of-plane deformation) of pyridine and pyrrole rings are observed at 814, 685 cm^{-1}, whereas these are calculated at 820, 766 cm^{-1}, respectively. The calculated wavenumber at 712 cm^{-1} displays the C—H wagging mode of benzene and it is observed at 610 cm^{-1} in the experimental FT-IR spectrum. The puckering vibrations (torsional modes) of benzene and pyridine rings are assigned at 689, 684 cm^{-1}, respectively.

4.6.3. C=O vibrations

The investigated molecule (**3**) contains two carbonyl groups as >C22=O23 and >C47=O48. The stretching vibration of hydrazide carbonyl group ($\nu_{C=O}$) is observed at 1656 cm^{-1}, whereas it is calculated at 1718 cm^{-1} in theoretical IR-spectrum. The observed wavenumber at 1656 cm^{-1} matches well with the reported C=O stretching vibration of —CONHR in literature in the region 1680–1640 cm^{-1} [72].

Table 4
Theoretical (selected) and experimental vibrational wavenumbers of (**3**) and their assignments: wavenumbers ($\bar{\nu}$/cm^{-1}), Intensity (K mmol^{-1}).

S. no.	$\bar{\nu}$ scaled	IR$_{int}$	$\bar{\nu}$ Exp.	Assignment (PED) ⩾ 5%
183	3506	56.43	3425	ν(N14H30)(99)
182	3492	62.8		ν(N39H55)(99)
181	3382	10.12	3286	ν(N21H34)(100)
180	3381	10.06		ν(N46H59)(100)
178	3136	4.48		ν(C41H56)(59) + ν(C42H57)(40)
177	3129	4.25		ν(C17H32)(86) – ν(C16H31)(13)
176	3122	6.12		ν(C42H57)(59) – ν(C41H56)(40)
173	3085	13.34		ν(C3H9)(45) + ν(C4H10)(26) + ν(C5H11)(19) + ν(C6H12)(8)
172	3078	31.27		ν(C3H9)(38) – ν(C5H11)(31) – ν(C6H12)(28)
171	3071	12.11		ν(C50H60)(90) + ν(C51H61)(9)
170	3070	12.02		ν(C25H35)(89) + ν(C26H36)(10)
169	3068	20.28		ν(C6H12)(39) – ν(C4H10)(28) – ν(C5H11)(11) + ν(C7H13)(10) + ν(C3H9)(10)
167	3049	31.51	3052	ν(C28H37)(93)
166	3049	31.07		ν(C53H62)(93)
164	3043	23.69		ν(C26H36)(87) – ν(C25H35)(9)
163	3042	25.98		ν(C51H61)(87) – ν(C50H60)(8)
162	2941	45.85	2923	ν(C19H33)(99)
161	2936	53.43		ν(C44H58)(99)
160	2910	9.95	2852	ν(C1H8)(99)
159	1718	427.68	1656	ν(C22O23)(59) – ν(C47O48)(18)
158	1717	71.95		ν(C47O48)(59) + ν(C22O23)(18)
157	1621	147.92	1602	ν(C19N20)(27) + ν(C44N45)(25) – ν(C18C19)(9) – ν(C43C44)(8) – (δip – C19H33)(7) – (δ-N45C44C43)(5)
155	1595	9.93		ν(C6C7)(22) + ν(C3C4)(21) + (δas-R1)(10) – ν(C2C3)(7) – ν(C2C7)(6) – (δ-C6H13C7)(6) + (δ-C2H9C3)(6)
154	1582	50.79		ν(C53C54)(11) + ν(C50C51)(10) + ν(C28C29)(10) + ν(C25C26)(9) – ν(C49C54)(5) + (δas-R2)(5) – ν(C24C29)(5)
153	1582	43.83		ν(C28C29)(11) + ν(C25C26)(10) – ν(C53C54)(10) – ν(C50C51)(9) – ν(C24C29)(5) + (δas-R2)(5)
149	1548	51.34		ν(C49C50)(17) – ν(C49C54)(15) + ν(N52C53)(10) – ν(C51N52)(10) – (δas-R2)(8) – ν(C24C25)(5)
147	1505	401.88		(δ-N46H59)(22) – (δ-N21H34)(22) + ν(N46C47)(7) + ν(N21C22)(7)
146	1503	443.53	1496	(δ-N21H34)(23) + (δ-N46H59)(22) + ν(N46C47)(7) – ν(N21C22)(7)
143	1472	21.74		(δ-N27H37C28)(12) + (δ-N27H36C26)(10) + (δ-C54H62C53)(9) + (δ-C50H61C51)(8) + (δ-C26H35C25)(6)
141	1455	46.13	1412	ν(C17C18)(7) + ν(C15C16)(7) + (δ-R)(6) – ν(C42C43)(6) – (δ-R)(6) – (ρ-N21H34)(6) + ν(C1C40)(5) – (ρ-N46H59)(5)
138	1408	21.16		ν(N14C18)(32) – (δ-C18H30N14)(14) – ν(N14C15)(12) + (δ-R)(11) – ν(C17C18)(10) + ν(C15C16)(7)
134	1392	15.62	1343	(δ-N27H36C26)(26) – (δ-N27H37C28)(21) + ν(C25C26)(15) – ν(C28C29)(15) – (δ-C26H35C25)(5) + (δ-C28H38C29)(5)
133	1317	31.15		(δ-N45C44C43)(27) – ν(C41C42)(11) + (δ-C41H57C42)(8) + ν(C44N45)(5) + ν(C43C44)(5)
132	1315	37.22	1287	($_{\delta\text{ip}}$-C19H33)(17) – ν(C16C17)(10) + (ρ-C1H8)(7) – (δ-C18H32C17)(6) – (δ-C6H13C7)(6) – (δ-C2H9C3)(6)
131	1312	13.00		(δ-C6H13C7)(18) + (δ-C2H9C3)(18)-(δ-C6H11C5)(9) – ν(C6C7)(6) + ν(C3C4)(5) – ν(C4C5)(5)
128	1302	7.4		(δ-C26H35C25)(17) – (δ-C28H38C29)(15) – (δ-N27H37C28)(10) + (δ-N27H36C26)(9)
127	1286	25.84		ν(C41C42)(21) + (δ-N45C44C43)(13) + (δ-C40H56C41)(10) + (δip-C43C44)(6) – ν(C1C40)(6) – (δip-C19H33)(5)
123	1249	30.11		(δ-C15C1C2)(19) – (δ-C18H30N14)(14) + (δ-C2C1C40)(11) + (δ-N45C44C43)(5)
122	1241	25.42		(ρ-C1H8)(16) – (δ-C15C1C40)(12) + ν(C2C3)(7) – ν(C1C2)(7) – (δ-C41H57C42)(7) + (δ-C40H55N39)(6)
121	1221	226.78		ν(C47C49)(27) – ν(N46C47)(14) + (ρ-N46H59)(11) – ν(C53C54)(8) + (δ-O48C47N46)(7) + (δtrigonal-R2)(5)
120	1220	308.7	1193	ν(C22C24)(27) – ν(N21C22)(14) – (ρ-N21H34)(11) – ν(C28C29)(8) + (δ-C22O23N21)(7) – ν(C241107C25)(6)
119	1204	76.94		(δ-C40H55N39)(12) + ν(C1C2)(9) – (δ-C18H32C17)(7) – (ρ-C1H8)(7) – (δ-C17H31C16)(6) – (δ-C41H57C42)(5)
117	1198	55.51		(δ-N27H36C26)(13) + (δ-N27H37C28)(10) – (δ-C28H38C29)(8) + ν(C26N27)(7) + ν(N27C28)(6)
116	1196	119.41		(δ-C15C1C2)(15) – (δ-C40H55N39)(11) – (δ-C18H32C17)(10) – (δ-C17H31C16)(10) + ν(C1C40)(6)
114	1162	36.18		(δ-C6H13C7)(11) + ν(C1C2)(9) – ν(C2C7)(8) + (δ-C40H56C41)(8) + (ρ-C1H8)(7) – (δ-C2H9C3)(7)
113	1148	94.54		ν(C1C2)(11) + (ρ-C1H8)(10) – ν(C2C7)(8) – (δ-C40H55N39)(7) + ν(C1C40)(6) + (δtrigonal-R1)(5)
112	1143	174.74	1127	(δ-C18H30N14)(17) – ν(N14C15)(12) + ν(N20N21) (10) + ν(C1C15)(6) + ν(C1C2)(5) + (δ-C15C1C2)(5) + (δ-R)(5)
110	1131	128.38		ν(N45N46)(23) – ν(N20N21)(13) – ν(N46C47)(8)
101	1029	51.51		(δ-C17H31C16)(29) – (δ-C18H32C17)(28) + ν(C16C17)(26)
100	1027	65.26	1012	(δ-C40H56C41)(29) – (δ-C41H57C42)(29) – ν(C41C42)(25)
93	972	13.46		ν(N39C40)(11) + ν(C1C40)(10) – (δ-R)(10) – (δ-R)(7) + (δ-C41H57C42)(6) + ν(C40C41)(5) – (δtrigonal-R2)(5)
84	914	9.69	910	(δoop-C19H33)(91)
81	888	16.62	843	(δ-C22O23N21)(27) – (δ-C22N21N20)(14) – (δtrigonal-R2)(10) + ν(C22C24)(8)
74	820	12.62	814	(ω-C25H35)(27) + (ω-C26H36)(15) – (δoop-C22C24)(10) + (δoop-C22C24)(9) – (ω-C28H37)(8)
70	766	60.04	685	(ω-C17H32)(39) + (ω-C16H31)(25)
69	764	33.51		(δ-R)(23) – (δ-C19N20C18)(14) + (δ-R)(6) – (ω-C17H32)(6) – (δ-C19N21N20)(6)
68	759	40.59		(ω-C41H56)(39) + (ω-C42H57)(32) – (ω-N39H55)(6) – (τ-R)(5)
64	712	38.97	610	(ω-C5H11)(18) + (R1-puckering)(14) – (ω-C7H13)(10) – (ω-C3H9)(9) + (ω-C6H12)(7)
59	666	49.18		(δas-R2)(28) + (δas-R2)(26) – (δ-O48C47N46)(5) – (δ-C22O23N21)(5) + ν(C47C49)(5)
58	665	59.31		(δas-R2)(27) – (δas-R2)(25) – (δ-C22O23N21)(5) + ν(C22C24)(5) + (δ-O48C47N46)(5)
50	584	22.6	567	(ω-N39H55)(33) + (τ-R)(23) + (δas-R1)(13) – (τ-R)(9)
49	550	49.24		(ω-N14H30)(64) + (τ-R)(17)
45	487	44.57		(ω-N46H59)(62) – (ω-N21H34)(18)
44	485	49.91		(ω-N21H34)(54) + (ω-N46H59)(13) – (τ-R1)(5)
41	420	8.72		(τ-R2)(17) – (τ-R2)(10)-(δoop-C22C24)(7) + (δ-C19N21N20)(6)

Proposed assignment and potential energy distribution (PED) for vibrational modes: Types of vibrations: ν-stretching, ρ-rocking, ω-wagging, δ-deformation, δs-symmetric deformation, δas-asymmetric deformation, δip-in plane deformation, δoop-out-of-plane deformation, τ-torsion. R-pyrrole ring, R1-benzene ring, R2-pyridine ring.

4.6.4. C—C vibrations

The calculated wavenumber at 1595 cm^{-1} exhibits the C═C stretches of benzene ring and corresponds to the observed band reported in literature in the region 1600–1585 cm^{-1} [71], 1630–1590 [72]. The C═C stretches in pyrrole ring are assigned at 1552 cm^{-1} and well corresponds to the observed wavenumber at 1550 cm^{-1}. The C═C stretches in pyridine ring are assigned at 1548 cm^{-1} in theoretical IR-spectrum. A combination band of $\nu_{C═C}$ in pyrrole ring and its deformation (δ-R) with 6% contribution in PED is calculated at 1455 cm^{-1}, whereas it is observed at 1412 cm^{-1} in the

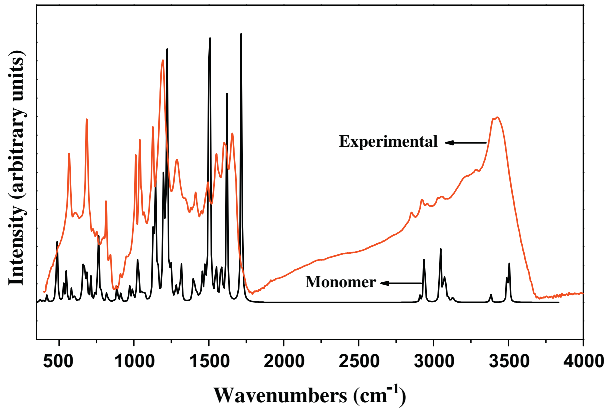

Fig. 4. Comparison between experimental and theoretical UV–Visible spectra for (**3**).

experimental FT-IR spectrum. The calculated wavenumber at 972 cm^{-1} exhibits presence of the C—C stretching vibration associated with C1 tetrahedral carbon atom (ν_{C1-C40}) and matches with the observed band for C—C= stretches reported in literature in the region 965–920 cm^{-1} [72]. The C—C stretching vibration ($\nu_{C22-C24}$) is calculated at 888 cm^{-1}, whereas it is observed at 843 cm^{-1} in the experimental FT-IR spectrum. The calculated wavenumber at 584 cm^{-1} exhibits the asymmetric deformation of benzene ring (δas-R1) with 13% contribution in PED and corresponds to the observed band at 567 cm^{-1} [71].

4.6.5. C—N and N—N vibrations

The observed C=N stretching vibration ($\nu_{C=N}$) at 1602 cm^{-1} agrees with the calculated wavenumber at 1621 cm^{-1} in theoretical IR spectrum. The presence of $\nu_{C=N}$ confirms the Schiff base (C=N) linkage in the product molecule (**3**). The observed $\nu_{C=N}$ at 1602 cm^{-1} also corresponds to the reported absorption band at 1600 cm^{-1} in literature [73]. The calculated wavenumber at 1220 cm^{-1} with 14% contribution in PED designates presence of the C—N stretching vibration ($\nu_{C22-N21}$) and corresponds to the observed wavenumber at 1193 cm^{-1} in the experimental FT-IR spectrum. The N—N stretching vibration ($\nu_{N20-N21}$) is calculated at 1143 cm^{-1} with 10% contribution in PED, whereas it is observed at 1127 cm^{-1} in the experimental FT-IR spectrum. The observed band at 1127 cm^{-1} is also in agreement with the reported band in literature at 1107 cm^{-1} [70].

4.7. Chemical reactivity

4.7.1. Global reactivity descriptors

The chemical reactivity and site selectivity of the molecular systems have been determined on the basis of Koopman's theorem [74]. The energies of frontier molecular orbitals (ε_{HOMO}, ε_{LUMO}), energy gap ($\varepsilon_{LUMO} - \varepsilon_{HOMO}$), electronegativity ($\chi$), chemical potential ($\mu$), global hardness ($\eta$), global softness ($S$), global electrophilicity index (ω) for (**1**), (**2**), (**3**) and ECT for reactant system [(**1**) ↔ (**2**)] are listed in Supplementary Table 4. The global elecrophilicity index (ω = 3.64 eV) for (**3**) shows that it behaves as a strong electrophile. Electrophilic charge transfer (ECT) = $(\Delta N_{max})_A - (\Delta N_{max})_B$ [75] is defined as the difference between the ΔN_{max} values of interacting molecules. If we consider two molecules A and B approach to each other (i) if ECT > 0, charge flow from B to A (ii) if ECT < 0, charge flow from A to B. ECT is calculated as 0.246 i.e. ECT > 0, for reactant system [(**1**) ↔ (**2**)], which indicates that charge flows from (**2**) to (**1**). Therefore, (**1**) acts as electron acceptor (electrophile) and (**2**) as electron donor (nucleophile).

4.7.2. Local reactivity descriptors

Selected nucleophilic reactivity descriptors (f_k^-, s_k^-, ω_k^-) for reactant (**1**), using Mulliken atomic charges are given in Supplementary Table 5. In reactant (**1**), the maximum values of the local nucleophilic reactivity descriptors (f_k^-, S_k^-, ω_k^-) at C2 indicate that this site is prone to electrophilic attack. It is to be noticed that the reactants (**2**), possess only one carbonyl functional group (>C=O), therefore for (**2**) there is no need to calculate the Local electrophilic reactivity descriptors (f_k^+, s_k^+, ω_k^+). Thus, Local reactivity descriptors for reactant (**1**) confirm the formation of product (**3**) by nucleophilic attack of the C2 carbon atom of (**1**) on the more electrophilic carbonyl carbon (C12) of the reactant (**2**). Selected electrophilic reactivity descriptors (f_k^+, s_k^+, ω_k^+) and nucleophilic reactivity descriptors (f_k^-, s_k^-, ω_k^-) for (**3**), using Hirshfeld charges are given in Supplementary Table 6. The maximum values of local electrophilic reactivity descriptors (f_k^+, s_k^+, ω_k^+) at Schiff base carbon (C19/C44) of (**3**) indicate that this site is more prone to nucleophilic attack and favor the formation of new heterocyclic compounds such as thiadiazoline, thiazolidinones and azetidinones by attack of nucleophilic part of the dipolar reagent on the carbon site of C=N bond.

4.8. Static dipole moment (μ_0), mean polarizability ($|\alpha_0|$), anisotropy of polarizability ($\Delta\alpha$) and first hyperpolarizability (β_0)

In order to investigate the relationship between molecular structure and NLO response, first hyperpolarizability (β_0) of this molecular system, and related properties ($|\alpha_0|$, $\Delta\alpha$) are calculated using B3LYP/6-31G(d,p), based on the finite-field approach and their calculated values are given in Supplementary Table 7. In the presence of an applied electric field, the energy of a system is a function of the electric field. First hyperpolarizability is a third rank tensor that can be described by a 3 × 3 × 3 matrix. The 27 components of the 3D-matrix can be reduced to 10 components due to the Kleinman symmetry [76–79]. It can be given in the lower tetrahedral format. It is obvious that the lower part of the 3 × 3 × 3 matrix is a tetrahedral. The components of μ, α, β are defined as the coefficients in the Taylor series expansion of the energy in the external electric field. When the external electric field is weak and homogeneous, this expansion of the energy in the external electric field is weak and homogeneous, this expansion becomes:

$$E = E^0 - \mu_a \sum E^a - 1/2\alpha_{ab} \sum E^a E^b - 1/6\beta_{abc} \sum E^a E^b E^c \\ - 1/24\gamma_{abcd} \sum E^a E^b E^c E^d - \ldots$$

where E^0 is the energy of the unperturbed molecules, E^a is the field at the origin, μ_a is component of the dipole moment and α_{ab}, β_{abc}, γ_{abcd} are the polarizability, first hyperpolarizability and second hyperpolarizability tensors, respectively. Large value of particular component of the polarizability and hyperpolarizability indicate a substantial delocalization of charge in these directions. The polarizabilities and hyperpolarizabilities characterize the response of a system in an applied electric field. Electric polarizability is a fundamental characteristic of atomic and molecular systems. The donor and acceptor substituents provide the requisite ground-state charge asymmetry, whereas the π-conjugation system provides a pathway for the redistribution of electric charges under the influence of electric fields. The first hyperpolarizability (β_0) of the title compound is calculated as 60.95 × 10^{-30} esu. In this study, *p*-Nitroaniline (*p*-NA) is chosen as a reference molecule because there were no experimental values for the title compound. The *p*-NA is one of the prototypical molecules used in the study of the NLO properties of molecular systems (for *p*-NA, β_0 = 11.54 × 10^{-30} esu). Therefore, investigated molecule will show non-linear optical response and might be used as non-linear optical (NLO) material.

5. Conclusions

The title compound (**3**) has been synthesized and characterized by experimental techniques and theoretical calculations. The calculated ^{1}H NMR chemical shifts are in agreement with the observed chemical shifts experimentally. A combined molecular orbital coefficients analysis and molecular orbital plots suggests that nature of both observed electronic excitations is $\pi \rightarrow \pi^*$. Natural bond orbitals (NBOs) analysis exhibits intramolecular conjugative interactions as $\pi \rightarrow \pi^*$, which are responsible for π-electron delocalization within pyrrole, benzene and pyridine rings. The intramolecular n_1 (N46) $\rightarrow \pi^*$(C47—O48) interaction stabilizes the molecule with maximum energy $\sim$216.61 kJ/mol. The local reactivity descriptors of reactant molecules confirm the formation of product molecule (**3**). The global electrophilicity index (ω = 3.64 eV) of (**3**) shows that product is electrophilic in nature. The electrophilic reactivity descriptors analysis of (**3**) indicates that the investigated molecule might be used as precursor for the target syntheses of new heterocyclic compounds such as thiadiazoline, thiazolidinones and azetidinones etc. The compound exhibits effective intramolecular charge transfer being responsible for hyperpolarisability. On the basis of first hyperpolarizability ($\beta_0 = 60.95 \times 10^{-30}$ esu), we conclude that title compound can be used as an attractive material for non-linear optical (NLO) applications.

Acknowledgement

Authors are thankful to the DST, New Delhi for providing the financial support.

Appendix A. Supplementary material

Supplementary data associated with this article can be found, in the online version, at http://dx.doi.org/10.1016/j.molstruc.2013.08.037.

References

[1] J.S. Lindsey, in: Metalloporphyrins Catalysed Oxidation, Kluwer Academic Publishers, The Netherlands, 1994, pp. 49–86.
[2] S.-J. Hong, M.-H. Lee, C.-H. Lee, Bull. Korean Chem. Soc. 25 (2004) 1545–1550.
[3] W.-S. Cho, H.-Je Kim, B.J. Littler, M.A. Miller, C.-H. Lee, J.S. Lindsey, J. Org. Chem. 64 (1999) 7890–7901.
[4] R.L. Halterman, X. Mei, Tetrahedron Lett. 37 (1996) 6291–6294.
[5] A. Jasat, D. Dolphin, Chem. Rev. (1997) 2277–2282.
[6] G. Mori, H. Shinokubo, A. Osuka, Tetrahedron Lett. 49 (2008) 2170–2172.
[7] R. Guilard, D.T. Gryko, G. Canard, J.-M. Barbe, B. Koszarna, S. Brande‘s, M. Tasior, Org. Lett. 4 (2002) 4491–4494.
[8] M. Schwalbe, D.K. Dogutan, S.A. Stoian, T.S. Teets, D.G. Nocera, Inorg. Chem. 50 (2011) 1368–1377.
[9] J.C. Wechsler, A.A.-S. Ali, E.E. Chapman, T.S. Cameron, A. Thompson, Inorg. Chem. 46 (2007) 10947–10949.
[10] L. Yu, K. Muthukumaran, I.V. Sazanovich, C. Kirmaier, E. Hindin, J.R. Diers, P.D. Boyle, D.F. Bocian, D. Holten, J.S. Lindsey, Inorg. Chem. 42 (2003) 6629–6647.
[11] C. Brückner, V. Karunaratne, S.J. Rettig, D. Dolphin, Can. J. Chem. 74 (1996) 2182–2193.
[12] S.-ichi Tamaru, L. Yu, W.J. Youngblood, K. Muthukumaran, M. Taniguchi, J.S. Lindsey, J. Org. Chem. 69 (2004) 765–777.
[13] A. Thompson, S.J. Retting, D. Dolphin, Chem. Commun. (1999) 631–632.
[14] S.M. Cohen, S.R. Halper, Inorg. Chim. Acta 341 (2002) 12–16.
[15] B. Moulton, M.J. Zaworotko, Chem. Rev. 101 (2001) 1629–1658.
[16] S.R. Halper, S.M. Cohen, Inorg. Chem. 44 (2005) 4139–4141.
[17] S.R. Halper, M.R. Malachowski, H.M. Delancy, S.M. Cohen, Inorg. Chem. 43 (2004) 1242–1245.
[18] L. Do, S.R. Halper, S.M. Cohen, Chem. Commun. (2004) 2662–2663.
[19] S.R. Halper, S.M. Cohen, Angew. Int. Ed. 43 (2004) 2385–2388.
[20] V.S. Thoi, J.R. Stork, D. Magde, S.M. Cohen, Inorg. Chem. 45 (2005) 10688–10697.
[21] S.R. Halper, L. Do, J.R. Stork, S.M. Cohen, J. Am. Chem. Soc. 128 (2006) 15255–15258.
[22] E.A. Katayev, N.V. Boev, V.N. Khrustalev, Y.A. Ustynyuk, Tananaev, J.L. Sessler, J. Org. Chem. 72 (2007) 2886–2896.
[23] S. Goeb, R. Ziessel, Tetrahedron Lett. 49 (2008) 2569–2574.
[24] A. Haefele, G. Ulrich, P. Retailleau, R. Ziessel, Tetrahedron Lett. 49 (2008) 3716–3721.
[25] K. Kim, C. Jo, S. Easwaramoorthi, J. Sung, D.H. Kim, D.G. Churchill, Inorg. Chem. 49 (2010) 4881–4894.
[26] S. Rollas, S.G. Küçükgüzel, Molecules 12 (2007) 1910–1939.
[27] F. Armbruster, U. Klingebiel, M. Noltemeyer, Z. Naturforsch. 61b (2006) 225–236.
[28] N. Ergenc, N.S. Gunay, Eur. J. Med. Chem. 33 (1998) 143–148.
[29] S. Gemma, G. Kukreja, C. Fattorusso, M. Persico, M.P. Romano, M. Altarelli, L. Savini, G. Campiani, E. Fattorusso, N. Basilico, D. Taramelli, V. Yardley, S. Butini, Bioorg. Med. Chem. Lett. 16 (2006) 5384–5388.
[30] E. Gursoy, N.G. Ulusoy, Eur. J. Med. Chem. 42 (2007) 320–326.
[31] A. Masunari, L.C. Tavaris, Bioorg. Med. Chem. 15 (2007) 4229–4236.
[32] M. Yu, H. Lin, H. Lin, Ind. J. Chem. Sec. A 46 (2007) 1437–1439.
[33] B. Szczesna, U. Lipkowska, Supramol. Chem. 13 (2001) 247–251.
[34] S. Vijayakumar, A. Adhikari, B. Kalluraya, K.N. Sharafudeen, K. Chandrasekharan, J. Appl. Polym. Sci. 119 (2011) 595–601.
[35] P.N. Prasad, D.J. Williams, Introduction to Nonlinear Optical Effects in Molecules and Polymers, Wiley, New York, 1991.
[36] F. Meyers, S.R. Marder, B.M. Pierce, J.L. Brédas, J. Am. Ceram. Soc. 116 (1994) 10703–10714.
[37] S.R. Marder, J.E. Sohn, G.D. Stucky, Materials for Nonlinear Optics: Chemical Perspectives, in: ACS Symposium Series, American Chemical Society, Washington DC, 1991.
[38] C. Bosshard, K. Sutter, P. Pretre, J. Hulliger, M. Florsheimer, P. Kaatz, P. Günter, Organic Nonlinear Optical Materials, Gordon & Breach, Basel, 1995.
[39] T.J. Marks, M.A. Ratner, Angew Chem. Int. Ed. Engl. 34 (1995) 155–173.
[40] R.G. Denning, J. Mater. Chem. 5 (1995) 365–378.
[41] S.R. Marder, B. Kippelen, A.K.-Y. Jen, N. Peyghambarian, Nature 388 (1997) 845–851.
[42] D. Cotter, R.J. Manning, K.J. Blow, A.D. Ellis, A.E. Kelly, D. Nesset, I.D. Phillips, A.J. Poustie, D.C. Rogers, Science 286 (1999) 1523–1528.
[43] M.J. Frisch, G.W. Trucks, H.B. Schlegel, G.E. Scuseria, M.A. Robb, J.R. Cheeseman, G. Scalmani, V. Barone, B. Mennucci, G.A. Petersson, H. Nakatsuji, M. Caricato, X. Li, H.P. Hratchian, A.F. Izmaylov, J. Bloino, G. Zheng, J.L. Sonnenberg, M. Hada, M. Ehara, K. Toyota, R. Fukuda, J. Hasegawa, M. Ishida, T. Nakajima, Y. Honda, O. Kitao, H. Nakai, T. Vreven, J.A. Montgomery, Jr., J.E. Peralta, F. Ogliaro, M. Bearpark, J.J. Heyd, E. Brothers, K.N. Kudin, V.N. Staroverov, T. Keith, R. Kobayashi, J. Normand, K. Raghavachari, A. Rendell, J.C. Burant, S.S. Iyengar, J. Tomasi, M. Cossi, N. Rega, J.M. Millam, M. Klene, J.E. Knox, J.B. Cross, V. Bakken, C. Adamo, J. Jaramillo, R. Gomperts, R.E. Stratmann, O. Yazyev, A.J. Austin, R. Cammi, C. Pomelli, J.W. Ochterski, R.L. Martin, K. Morokuma, V.G. Zakrzewski, G.A. Voth, P. Salvador, J.J. Dannenberg, S. Dapprich, A.D. Daniels, O. Farkas, J.B. Foresman, J.V. Ortiz, J. Cioslowski, D.J. Fox, Gaussian 09, Revision B.01, Gaussian, Inc., Wallingford, CT, 2010.
[44] A.D. Becke, J. Chem. Phys. 98 (1993) 5648–5652.
[45] C.T. Lee, W.T. Yang, R.G.B. Parr, Phys. Rev. 37 (1988) 785–789.
[46] D.A. Petersson, M.A. Allaham, J. Chem. Phys. 94 (1991) 6081–6090.
[47] G.A. Petersson, A. Bennett, T.G. Tensfeldt, M.A. Allaham, W.A.J. Mantzaris, G.A. Petersson, Andrew Bennett, Thomas G. Tensfeldt, Mohammad A. Al-Laham, William A. Shirley, John Mantzaris, J. Chem. Phys. 89 (1988) 2193–2218.
[48] M. Sarafran, A. Komasa, E.B. Adamska, J. Mol. Struct. 827 (2007) 101–107.
[49] A.E. Reed, L.A. Curtiss, F. Weinhold, Chem. Rev. 88 (1988) 889–926.
[50] C.G. Liu, Z.M. Su, X.H. Guan, S. Muhammad, J. Phys. Chem. C 115 (2011) 23946–23954.
[51] J.M.L. Martin, V. Alsenoy, C.V. Alsenoy, Gar2ped software, University of Antwerp, 1995.
[52] R.G. Pearson, J. Org. Chem. 54 (1989) 1430–1432.
[53] R.G. Parr, R.G. Pearson, J. Am. Chem. Soc 105 (1983) 7512–7516.
[54] P. Geerlings, F.D. Proft, W. Langenaeker, Chem. Rev. 103 (2003) 1793–1874.
[55] R.G. Parr, L. Szentpály, S. Liu, J. Am. Chem. Soc. 121 (1999) 1922–1924.
[56] P.K. Chattaraj, U. Sarkar, D.R. Roy, Chem. Rev. 106 (2006) 2065–2091.
[57] D. Avci, Spectrochim. Acta A 82 (2011) 37–43.
[58] D. Avci, A. Başoğlu, Y. Atalay, Struct. Chem. 21 (2010) 213–219.
[59] D. Avci, H. Cömert, Y. Atalay, J. Mol. Model. 14 (2008) 161–169.
[60] N. Sundaraganesan, E. Kavitha, S. Sebastian, J.P. Cornard, M. Martel, Spectrochimica Acta Part A 74 (2009) 788–797.
[61] G.K. Patra, Y.D. Posner, I. Goldberg, Acta Cryst. E58 (2002) o530–o531.
[62] N. Maiti, J. Lee, D.G. Churchill, Y. Do, H.S. Shin, J. Chem. Crystallography 35 (2005) 949–955.
[63] S.M.S.V. Wardel, J.L. Wardel, M.V.N. de Souza, J.N. Low, C. Glidewel, Acta Cryst. C62 (2006) o47–o49.
[64] M.V.N. de Souza, J.L. Wardell, S.M.S.V. Wardell, J.N. Low, C. Glidewel, Acta Cryst. C63 (2007) o166–o168.
[65] K. Wolinski, J.F. Hinton, J.F. Pulay, J. Am. Chem. Soc. 112 (1990) 8251–8260.
[66] J. P Foster, F. Weinhold, J. Am. Chem. Soc. 102 (1980) 7211–7218.
[67] F. Weinhold, C.R. Landis, Valency and Bonding: a Natural Bond Orbital Donor–Acceptor Perspective, Cambridge University Press, Cambridge, New York, Melbourr, 2005.
[68] J.A. Pople, H.B. Schlegel, R. Krishnan, D.J. Defrees, J.S. Binkley, M.J. Frisch, R.A. Whiteside, R.F. Hout, W.J. Hehre, Int. J. Quantum Chem. 15 (1981) 269–278.
[69] B.M. Giuliano, I. Reva, R. Fausto, J. Phys. Chem. A 114 (2010) 2506–2517.
[70] M.R. Anoop, P.S. Binil, S. Suma, M.R. Sundarsanakumar, S. Mary, H.T. Varghese, C.Y. Panicker, J. Mol. Struct. 969 (2010) 48–54.
[71] R.M. Silverstein, F.X. Webster, Spectrometric Identification of Organic Compounds, sixth ed., Jon Wiley Sons Inc., New York, 1963. pp. 72–108.

[72] J.B. Lambert, H.F. Shurvell, Lawrence Verbit, R.G. Cooker, G.H. Stout, Organic Structural Analysis, 2009, pp. 235 (Chapter 4).

[73] J.E. Mostapha, A. Riou, M. Allain, M.A. Khan, G.M. Bouet, Polyhedron 20 (2001) 67–74.

[74] R.G. Parr, W. Yang, Density functional Theory of Atoms and Molecules, Oxford University Press, Oxford, New York, 1989.

[75] J. Padmanabhan, R. Parthasarathi, V. Subramaniaan, P.K. Chattaraj, J. Phys. Chem. A 111 (2007) 1358–1361.

[76] C.R. Zhang, H.S. Chen, G.H. Wang, Chem. Res. Chin. U 20 (2004) 640–646.

[77] Y. Sun, X. Chen, L. Sun, X. Guo, W. Lu, Chem. Phys. Lett. 381 (2003) 397–403.

[78] O. Christiansen, J. Gauss, J.F. Stanton, Chem. Phys. Lett. 305 (1999) 147–155.

[79] D.A. Kleinmann, Phys. Rev. 126 (1962) 1977–1979.